Article:

Unequal order T-spline meshes for fracture in poroelastic media

Tim Hageman [ID][1] and René de Borst [ID][1,*]

[1]Department of Civil and Structural Engineering, University of Sheffield, Sheffield, UK

*Corresponding author: r.deborst@sheffield.ac.uk

ABSTRACT

Spline-based meshes allow for a higher inter-element continuity. For coupled problems, e.g. poroelasticity, different meshes with different orders of interpolation are normally used for the various fields in order to avoid spurious oscillations. When including discontinuities in these meshes, there exist several options for the discretisation. Herein we will discuss two options which use T-splines, one aiming at a minimum number of degrees of freedom around the crack tip, the other trying to maximise this number. Both meshes retain a higher-order continuity along the fracture, but the mesh which maximises the number of degrees of freedom mesh introduces two additional degrees of freedom around the crack tip to allow for a sharper crack. The two discretisations are used to simulate a pressurised fracture inside a poroelastic material and the results are compared to results obtained using a Non-Uniform Rational B-Spline (NURBS) mesh. A comparison between the two discretisations shows the effect of including additional degrees of freedom close to the crack tip. However, both meshes yield similar results further away from the crack tip. It is shown that both T-spline meshes capture a fully closed discontinuity at the fracture tip, whereas the NURBS mesh retains a small opening due to the discontinuity which exists for the cracked as well as the intact elements. A fully closed fracture aperture results in T-splines with a lower discontinuity pressure compared to NURBS, making T-splines more suitable for simulations in which the fracture propagation is limited by the fluid transport within the fracture.

KEYWORDS: T-splines, isogeometric analysis, fracture, poroelasticity

1. INTRODUCTION

An advantage of using spline-based interpolation functions compared to standard Lagrangian polynomials is their increased inter-element continuity. When simulating fluid flows within poroelastic materials, this increased continuity allows for continuous fluid fluxes between the elements [1], thereby fulfilling conservation of mass not just on a per-element basis, but also locally across element boundaries. Moreover, this increased continuity allows for more advanced models for the simulation of fluid flows within fractures [2], since the fluid velocity is continuous rather than discontinuous as would be the case when using standard Lagrangian polynomials.

Poroelastic problems are typically solved using a displacement-pressure ($u - p$) formulation. A requirement is then that the Ladyzhenskaya–Babuška–Brezzi (or inf-sup) condition [3–5] is satisfied, which typically results in the use of unequal order meshes to prevent spurious oscillations [6]. Similar oscillations are encountered in other fields, e.g. fluid mechanics, when equal-order meshes are used for the pressure and the velocity [7, 8]. While it is possible that these oscillations do not occur when using equal order meshes, they tend to dominate the solution when they occur. This necessitates the use of complex stabilisation schemes to retain usable results when using the same interpolants for the displacements and pressure [9–11]. Non-Uniform Rational B-Splines (NURBS)

meshes using different interpolation function orders for the displacements and pressures can be easily generated through p-refinement [12]. This ease of generating unequal order meshes makes NURBS well-suited for the simulation of coupled problems such as poroelasticity.

NURBS are defined using global knot vectors, allowing for smaller and deformed elements only if the number of elements in the horizontal and vertical directions remains constant. As a result, mesh refinement near areas of interest is normally not possible without introducing new elements throughout the domain. Furthermore, when simulating fractures using interface elements they need to be inserted along a line crossing the entire domain. This creates further issues, requiring a dummy stiffness and lumped integration schemes to be used to prevent traction and fracture inflow oscillations [13, 14]. Furthermore, special integration schemes are needed near the fracture tip to prevent non-physical amounts of fluid from entering the fracture [14].

There exist spline discretisation schemes which allow for mesh refinement. Hierarchical NURBS permit smaller elements to be used near areas of interest [15, 16], but do not allow for a single interface element to be inserted to propagate a fracture [17]. T-splines also allow for mesh refinement [18–21], and also make it possible to insert single interface elements [22, 23].

In this paper, we will describe how to generate meshes of unequal order T-splines which include discontinuities. The
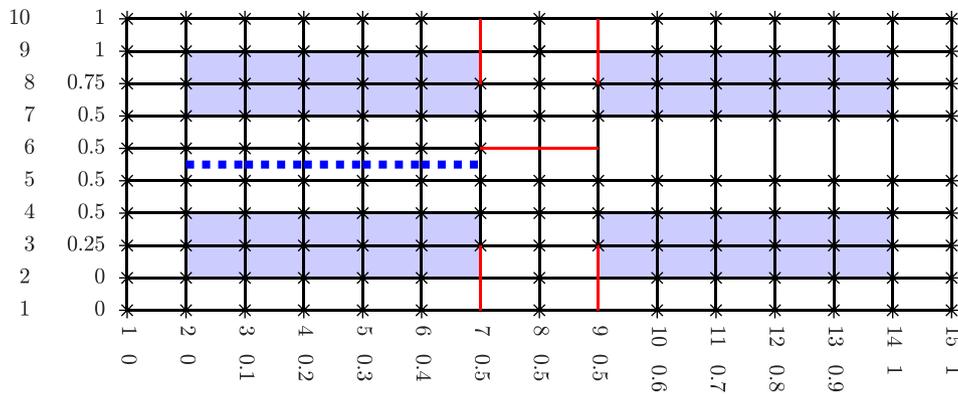
(a) C^0 continuity lines normal to the discontinuity.
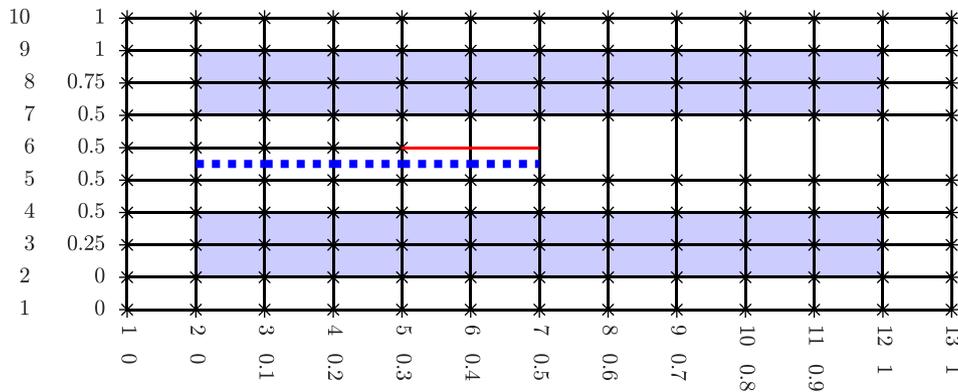
(b) Discontinuity composed of meshlines and reduced continuity lines.

Figure 1 Possibilities to create interface elements for a cubic mesh in index (outer coordinate numbering) and parametric (inner coordinate numbering) spaces. Black lines are meshlines, red lines are reduced continuity lines, markers are control points/anchors, blue squares are elements and dotted lines are interface elements.

use of T-splines allows for several options with regard to the representation of discontinuities, of which two possible discretisation options are explored. These two meshes are used to simulate a typical poroelasticity case, and their results are compared to a discretisation using NURBS, showing the impact of the different discretisation choices, and highlighting the advantages of T-splines.

2. MESH GENERATION

T-spline meshes are defined through a T-mesh, given in an index/parametric space [18]. On this mesh, the anchors correspond to control points in the physical space. These anchors each have their own local knot vector, which are defined through the mesh lines. An example of a T-mesh in index space is given in Fig. 1. By having multiple mesh lines in the index space corresponding to the same value in the parametric space, knots are repeated and the continuity is reduced at the location of the repeated knots [24]. Since the mesh lines for T-meshes are allowed to start and stop at each perpendicular mesh line, a C^{-1} continuity can be inserted between elements to represent a fracture without creating a C^{-1} continuity between elements that do not represent the fracture, which is different from NURBS.

The shape functions created through the knot vectors occupy a square spanned by these knot vectors. This introduces a reduced continuity at the edge of the space occupied by the shape function. For most cases, this reduced continuity coincides with a mesh line, which were inserted on purpose to create this reduced continuity. However, when mesh lines terminate, the shape functions using those mesh lines will create additional reduced continuity lines, as shown in Fig. 1. To use T-splines in a similar manner as NURBS and standard Lagrangian finite elements, elements are defined on the T-mesh. These elements are enclosed by the combination of mesh lines and reduced continuity lines, creating an element when a non-zero area is covered in the parametric space [25]. Similarly, interface elements are created when a non-zero length is covered by the mesh lines and reduced continuity lines together representing a C^{-1} continuity [24].

This makes it possible to choose how the interface elements are used to represent the fracture. The approach taken by [22–24] is to isolate the fracture from the still-to-fracture part by inserting a C^0 continuity line perpendicular to the fracture, as shown in Fig. 1a. Interface elements only correspond to the mesh lines, while the reduced continuity lines are contained by the C^0 continuity line. When the fracture is propagated, the reduced continuity is left in place, resulting in a reduced continuity in between the interface elements.

(a) "Correct" use of 3 refinement layers around the discontinuity.

(b) "Incorrect" use of 2 refinement layers around the discontinuity.
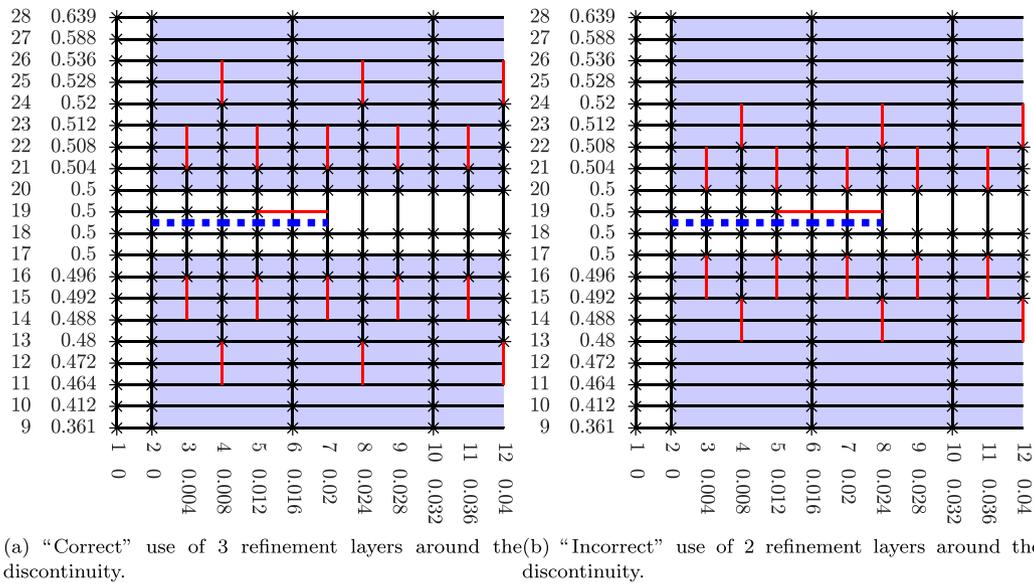
Figure 2 Example of mesh refinement layers for a cubic mesh. Black lines are meshlines, red lines are reduced continuity lines, markers are control points/anchors, blue squares are elements, and dotted lines are interface elements.

(a) Minimal amount of discontinuity lines.

(b) Maximum amount of discontinuity lines.
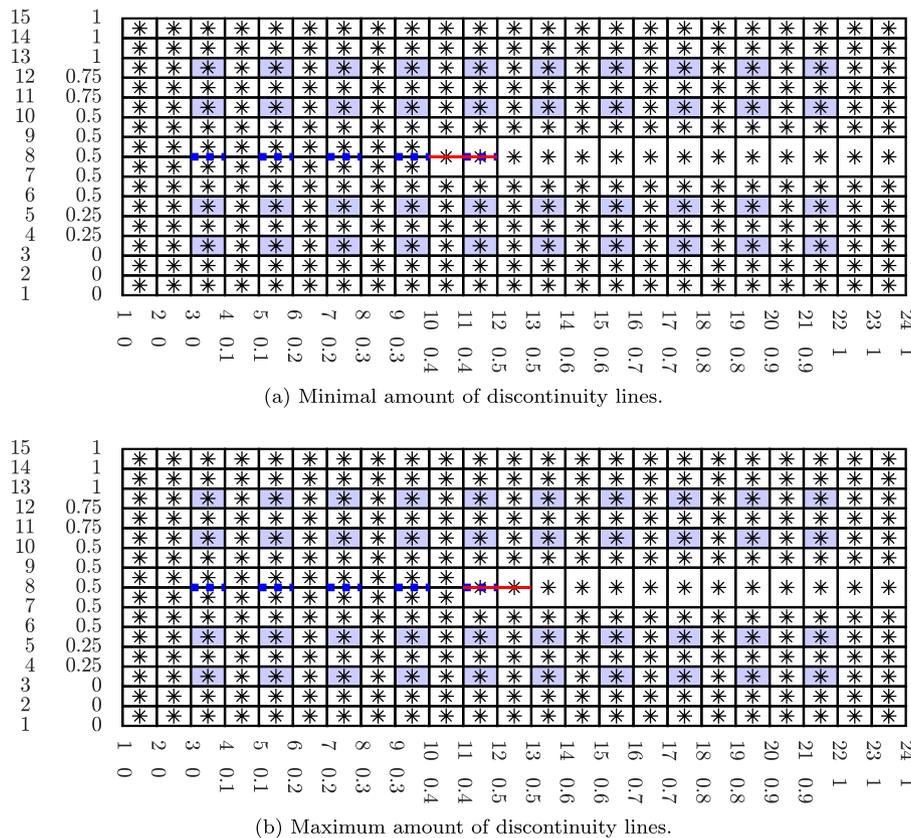
Figure 3 Possibilities to create interface elements for a quartic mesh, compatible with the mesh from Fig. 1b.

An alternative approach is to insert interface elements at the mesh lines and reduced continuity lines, as shown in Fig. 1b. This has as major advantage that the higher-order continuity is preserved, both around the fracture tip in the porous material and between the interface elements at the fracture. However, this lim-its the number of shape functions near the crack tip, slightly re-ducing the possibility to represent the interstitial pressure jump close to the crack tip. This disadvantage is smaller when finer meshes are used, but the reduced continuity resulting from the first approach remains. Therefore, the second approach will be

used as it will result in a continuous fluid velocity within the fracture.

For mesh refinements near the discontinuity and areas of interest a similar consideration is possible. Either isolate the different refinement layers with C^0 continuity layers, or utilise reduced continuity lines to define some of the smaller elements. While complicating the mesh generation, the last option preserves the higher inter-element continuity and is therefore used here, with an example of the refinement layers shown in Fig. 2a. It should be noted that care has to be taken when combining mesh refinement layers with interface elements. For a cubic mesh, layers of at least three small elements need to surround the discontinuity to isolate the discontinuity from the coarser elements. For example, the interface elements defined through reduced continuity lines are defined through the anchor at $(4,21)$ and $(5,21)$ (among others). If only a 2-element refinement layer were used, Fig. 2b, the anchor at $(4,21)$ would suddenly use the coarser element size to create reduced continuity lines at the discontinuity, forcing the discontinuity to propagate two interface elements at a time.

2.1. Unequal order meshes

Next to a cubic mesh for the interstitial fluid pressure, a quartic mesh is needed for the solid displacement. This quartic mesh needs to represent the exact same geometry and elements as the cubic mesh to enable the coupling between the solid and fluid. Therefore, the quartic mesh requires the same inter-element continuity as the cubic mesh, and thus requires additional mesh lines such that every mesh line and reduced continuity line is repeated once.

Since reduced continuity lines for both quartic and cubic meshes have the same length in the index space, and since each mesh line is repeated for the quartic mesh, the reduced continuity lines have different lengths in the parametric (and therefore in the physical) space. Cubic meshes contain two additional interface elements due to these reduced continuity lines, as shown in Fig. 1b, whereas only a single additional interface element is created for the quartic mesh, Fig. 3. This is resolved by inserting additional mesh lines at the discontinuity, resulting in equal discontinuity length for the quartic and cubic meshes.

The discontinuity near the fracture tip is allowed to contain an extra mesh line, as shown in Fig. 3. While this extra mesh line does not add an extra interface element due to the repeated knot, it does add an extra control point for the quartic mesh. This introduces an extra interpolation function, as shown in Fig. 4, and allows for a sharper fracture tip. Both meshes in the parametric space result in the same mesh and interface elements in the physical space. In the next section, the effect of this choice on the resulting fracture opening will be analysed.

Similar issues arise for mesh refinement, as shown in Figs. 9 and 10. Additional mesh lines now need to be inserted tangentially to the refinement layer in order to match the elements and inter-element continuity between the meshes. The repeated mesh lines in the parametric space offer a choice at this point, allowing for an extra layer of anchors/mesh lines to be inserted while still corresponding to the discretisation of the cubic mesh. Herein, the choice has been made to use a minimum
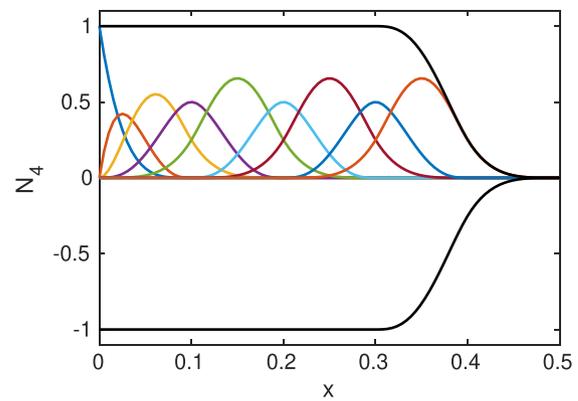
(a) Minimal amount of discontinuity lines (Figure 3a).
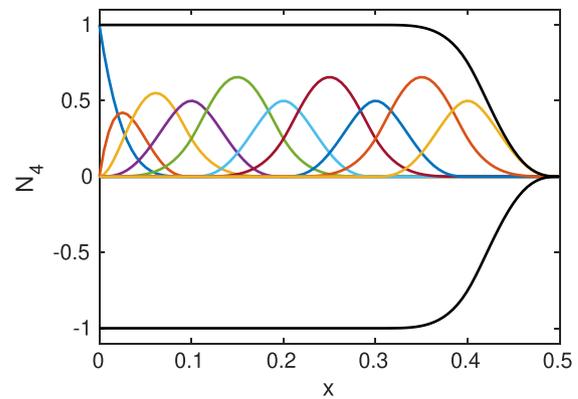
(b) Maximum amount of discontinuity lines (Figure 3b).
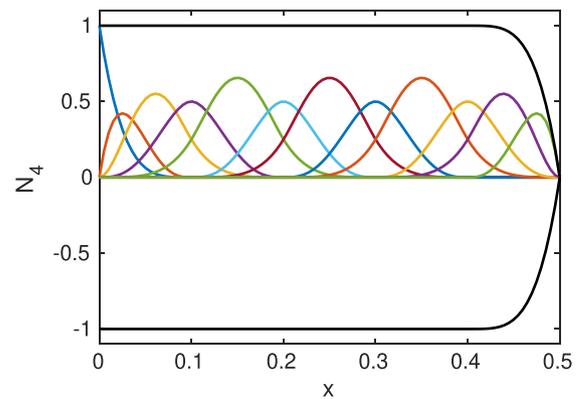
(c) C^0 continuity line at fracture tip (not used)

Figure 4 Discontinuous interpolants at the interface, and values across the discontinuity by imposing -1, 1 at all control points. Results use the parametric coordinate x, corresponding to the horizontal axis in the referenced figures.

required number of anchors instead of using an additional layer, mainly to limit the number of degrees of freedom associated with the solid displacement (which has much more anchors/control points due to the repeated mesh lines).

2.2. Discontinuity specific degrees of freedom

When simulating pressurised fractures, the pressure inside the fracture is defined through separate degrees of freedom, which are solely defined on the discontinuity. If these degrees of freedom were solely added to the discontinuous control points, the
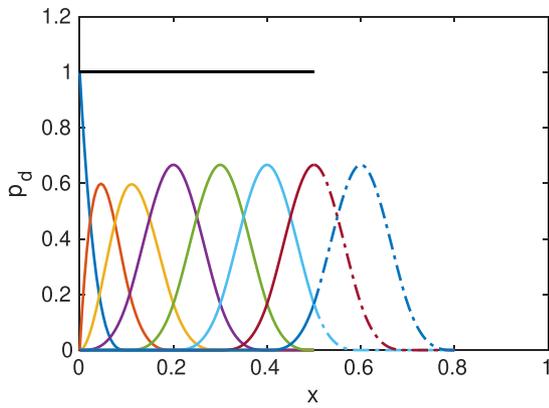
Figure 5 Example of the interpolants used for the discontinuity pressure.

pressure at the fracture tip would be forced to be equal zero. To allow the fracture pressure at the fracture tip to be non-zero, discontinuity pressure degrees of freedom are added to all the control points located at the bottom of the interface elements, irrespective whether they are duplicated with a top node to create a C^{-1} discontinuity or are still C^0 continuous. The parts of the interpolation functions that are not contained within an interface element are disregarded, and are only included when the fracture propagates to create new interface elements covering their length. The resulting interpolation functions and the " ignored" parts of these functions are shown in Fig. 5.

2.3. Fracture propagation

The fracture is propagated by creating new interface elements through mesh line insertions, as shown in Fig. 6. To limit remeshing, a C^0 continuity line is inserted at the future fracture path when the mesh is generated. This simplifies mesh line insertion, since only the location of the anchors in the parametric space is changed, but not the location of the control points in the physical space. The Bézier extraction operators for the interior elements are not changed by propagating the fracture along the pre-inserted C^0 continuity line. Furthermore, the Bézier extractor for the newly created interface elements can be directly taken from the neighbouring interior elements.

The discontinuity inside the cubic mesh is propagated by inserting a single mesh line one interface element behind the fracture tip, as shown in Fig. 6a. This creates a new anchor at the end of this mesh line and creates a new interface element to propagate the fracture. The control point corresponding to this newly created anchor is initialised by setting the displacements and interstitial fluid pressure equal to the pre-existing control point at the same location, now belonging to the bottom of the discontinuity. A similar procedure is applied to the quartic meshes, where inserting two mesh lines and two anchors creates a single new interface element and two new control points, as shown in Fig. 6b.

3. POROELASTICITY

To compare the different meshes, a poroelastic case is simulated. The porous material is governed by the momentum balance of
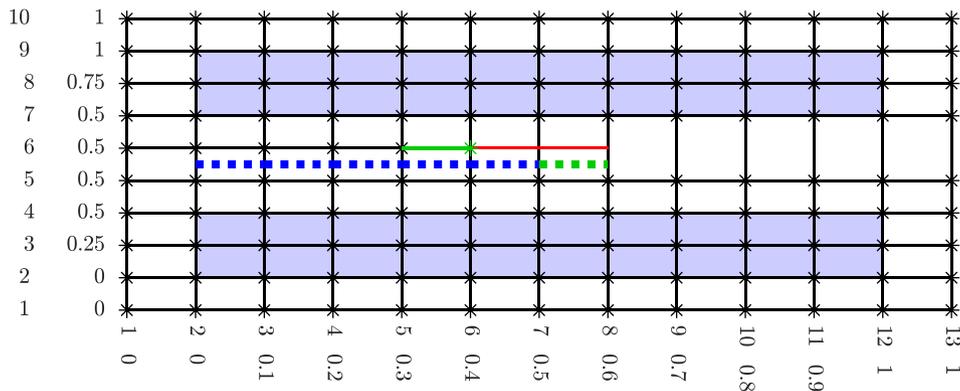
(a) Cubic mesh.
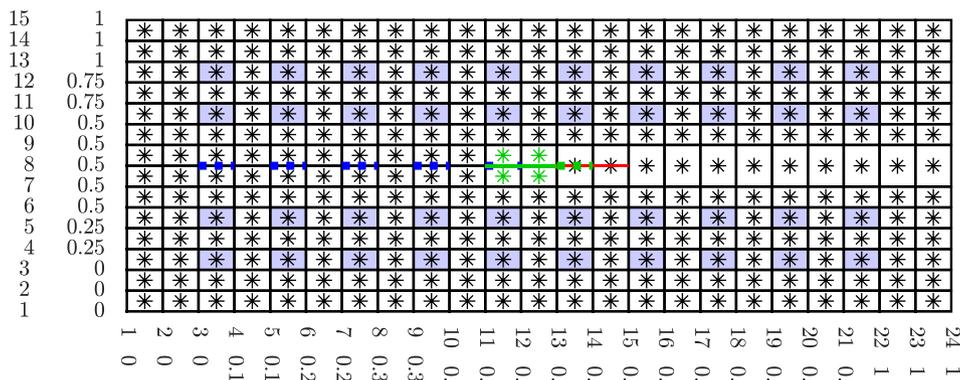
(b) Quartic mesh.

Figure 6 Fracture propagation by inserting the green mesh lines for the cubic and quartic meshes from Figs. 1b and 3b.
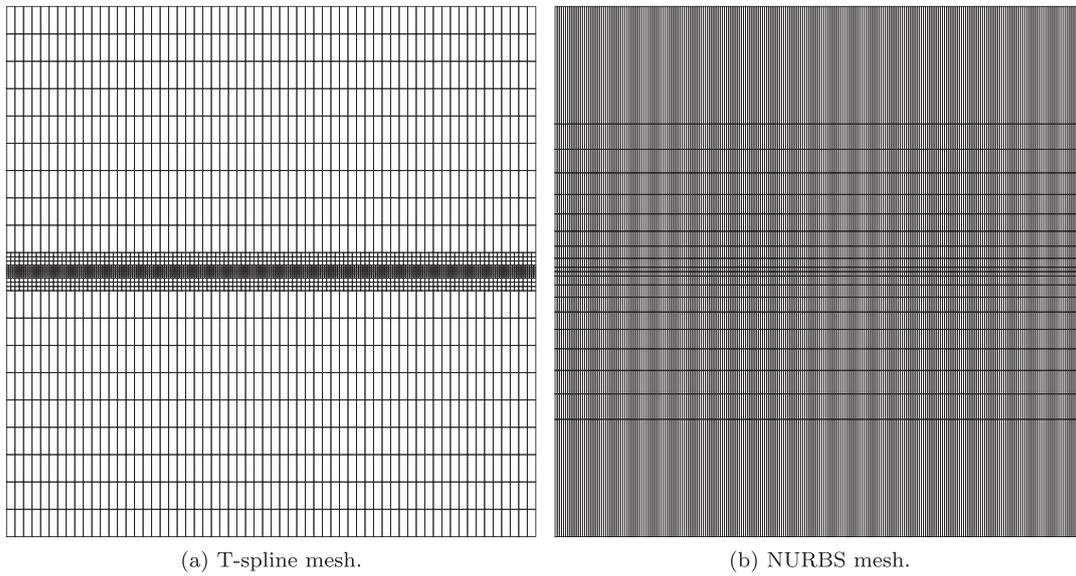
(a) T-spline mesh.

(b) NURBS mesh.

Figure 7 T-spline and NURBS meshes used for the example case in physical space.

the combined solid and fluid [26, 27]:

$$\nabla \cdot (\boldsymbol{\sigma}_s - \alpha p \mathbf{I}) = \mathbf{0}, \tag{1}$$

using the linear-elastic stresses in the porous solid $\boldsymbol{\sigma}_s$, the interstitial fluid pressure p and the Biot coefficient α. In addition, the mass balance for a Newtonian fluid is given by:

$$\frac{1}{M}\dot{p} + \alpha \nabla \cdot \dot{\boldsymbol{u}} + \nabla \cdot \left(-\frac{k}{\mu}\nabla p\right) = 0, \tag{2}$$

with Biot modulus M, intrinsic permeability k and fluid viscosity μ. The boundary conditions for these equations are given for the external boundaries Γ by:

$$\boldsymbol{u} = \bar{\boldsymbol{u}} \quad or \quad \boldsymbol{\sigma}_s \cdot \boldsymbol{n} = \bar{\boldsymbol{\tau}}, \tag{3}$$

$$p = \bar{p} \quad or \quad -\frac{k}{\mu}\nabla p \cdot \boldsymbol{n} = \bar{q}, \tag{4}$$

using the prescribed displacements and pressures $\bar{\boldsymbol{u}}$ and $\bar{p}$, respectively, and the prescribed tractions and fluid inflows, $\bar{\boldsymbol{\tau}}$ and $\bar{q}$, respectively. The tractions at the discontinuity Γ_d are governed by:

$$\boldsymbol{\tau}_d = \boldsymbol{\tau}_s([[\boldsymbol{u}]]) - p_d \boldsymbol{n}_d, \tag{5}$$

using an exponential traction-separation law to relate the displacement jump $[[\boldsymbol{u}]]$ to the solid interface traction $\boldsymbol{\tau}_s$. The fluid pressure within the fracture, p_d, is treated as an independent degree of freedom, resulting in a discontinuous pressure model being used for the fracture [14, 28]. This allows the fracture inflow on Γ_d to be given by:

$$q_d = k_i (p - p_d), \tag{6}$$

using a constant interface permeability k_i. This is appended with the mass balance within the fracture:

$$k_i(2p_d - p^+ - p^-) - \frac{\partial}{\partial x_d}\left(\frac{(\boldsymbol{n}_d \cdot [[\boldsymbol{u}]])^3}{12\mu}\frac{p_d}{\partial x_d}\right) + \frac{\boldsymbol{n}_d \cdot [[\boldsymbol{u}]]}{\partial t} = 0, \tag{7}$$

with the gradients of the pressure determined along the fracture in the fracture-local coordinate x_d.

These equations allow for a poroelastic material to be described using the interstitial and discontinuity pressures, and the solid displacement. Both pressures are discretised using cubic T-splines, with the interstitial fluid pressure discretised on the complete domain while the discontinuity pressure is solely represented on the discontinuity. The displacements are discretised using quartic T-splines, in an attempt to satisfy the inf-sup condition and to prevent possible non-physical oscillations.

4. EXAMPLE

We simulate a typical hydraulic fracturing case consisting of a square 0.25 m × 0.25 m domain, with an initial fracture of $L_{frac} = 5$ mm at the centre of the left boundary as shown in Fig. 8. A fluid inflow $Q_{in} = 10^{-5}$ m^2/s is imposed on the left, with this fluid inflow driving the fracture along a horizontal C^0 continuity line. The solid material is characterised through a Young's modulus $E = 25.85$ GPa, a Poisson ratio $\nu = 0.18$ and a bulk modulus $K_s = 13.46$ GPa. A water-like fluid is simulated, using a viscosity $\mu = 0.5$ mPa s and a bulk modulus $K_f = 0.2$ GPa. The fracture is characterised through an exponential traction-separation law, using a tensile strength $f_t = 1.7$ MPa and a fracture energy $\mathcal{G}_c = 0.2$ kN/m, and a constant interface permeability $k_i = 10^{-10}$ m/Pa s to govern the fracture outflow. Finally, three different intrinsic permeabilities are used for the porous material, $k = 10^{-16}$ m^2, $k = 10^{-17}$ m^2 and $k = 10^{-18}$ m^2, respectively, allowing to investigate the influence of fluid leak-off.

The domain is discretised using three distinct layers of elements: 248 × 6 square elements near the discontinuity (with the elements slightly deformed such that the initial discontinuity length corresponds to 5 elements), surrounded by layers of 124 × 3 and 62 × 9 elements, as shown in Fig. 7a. The resulting cubic mesh used for the fluid is shown in Fig. 2, and the
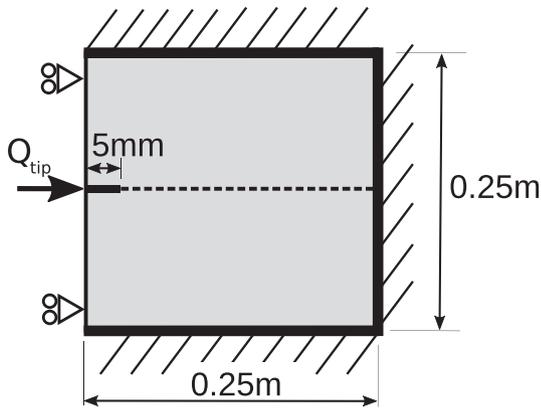
Figure 8 Geometry used for the poroelastic example case.

two quartic meshes used for the solid displacement are shown in Fig. 9 for the mesh using the minimum amount of degrees of freedom at the fracture tip, and Fig. 10 for the maximum amount. These meshes result in a total of 29 782 and 29 784 degrees of freedom before fracture propagation, respectively. The temporal discretisation has been done through an Euler backward scheme, using a constant time step $\Delta t = 1$ ms. The results are compared with the NURBS-based solution from [14], which used 250 ×

20 rectangular elements with a total of 52 854 degrees of freedom (Fig. 7b).

4.1. Results

The fracture propagation is shown in Fig. 11 for the two T-spline meshes and for the NURBS reference case. The two T-spline meshes result in the same fracture length, while the NURBS mesh matches for the high permeability, but is a few elements ahead for the medium and lower permeabilities.

The fracture aperture, Figs. 12 and 13, shows the influence of the interpolants near the fracture tip. Both T-spline meshes result in a fracture opening height that approaches zero at the fracture tip, with the mesh with the maximum number of discontinuity lines resulting in a slightly higher opening within the two closest elements to the tip. The NURBS mesh, however, yields a small displacement jump ahead of the fracture tip in the still intact material. This is caused by the interface elements having been inserted for the fractured and the not yet fractured elements, the used dummy stiffness not being able to completely enforce a closed fracture at the fracture tip.

These differences in fracture aperture influence the pressure within the discontinuity, Fig. 14. The T-spline meshes result in similar values for the pressure, indicating that the minor
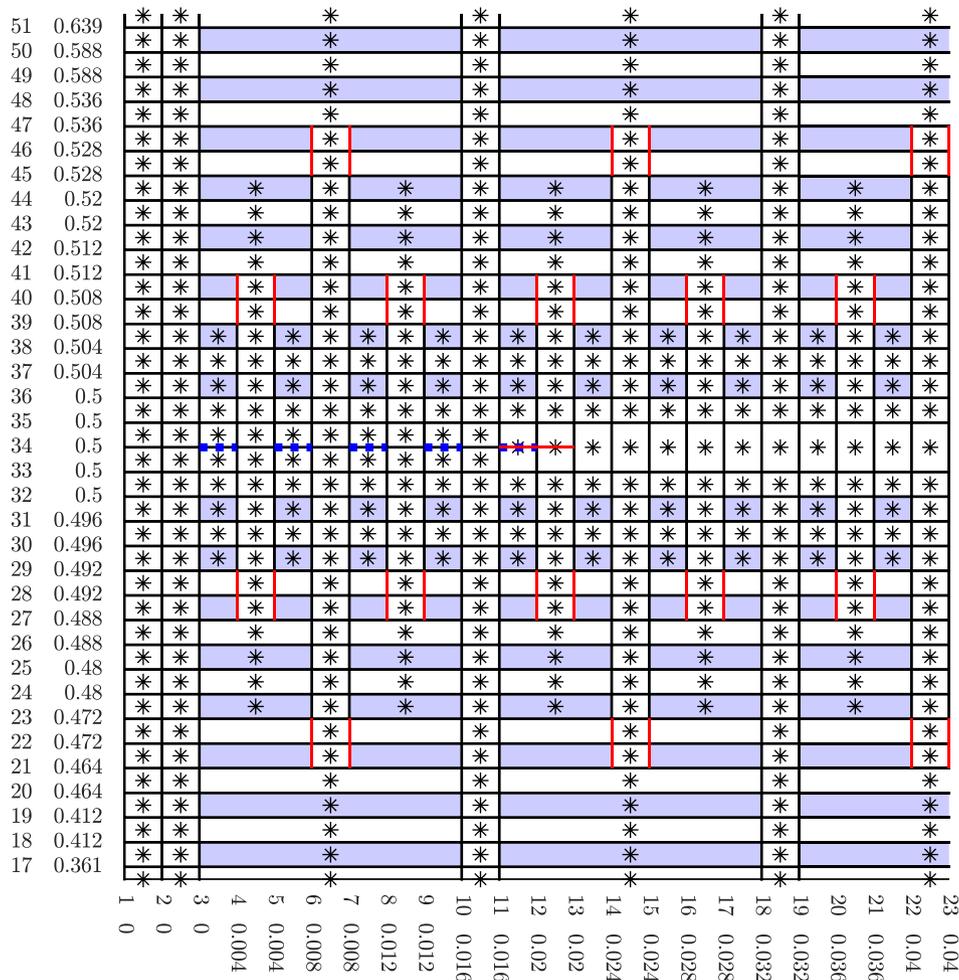
Figure 9 Quartic mesh using the minimum amount of discontinuity lines, as used for the example case.
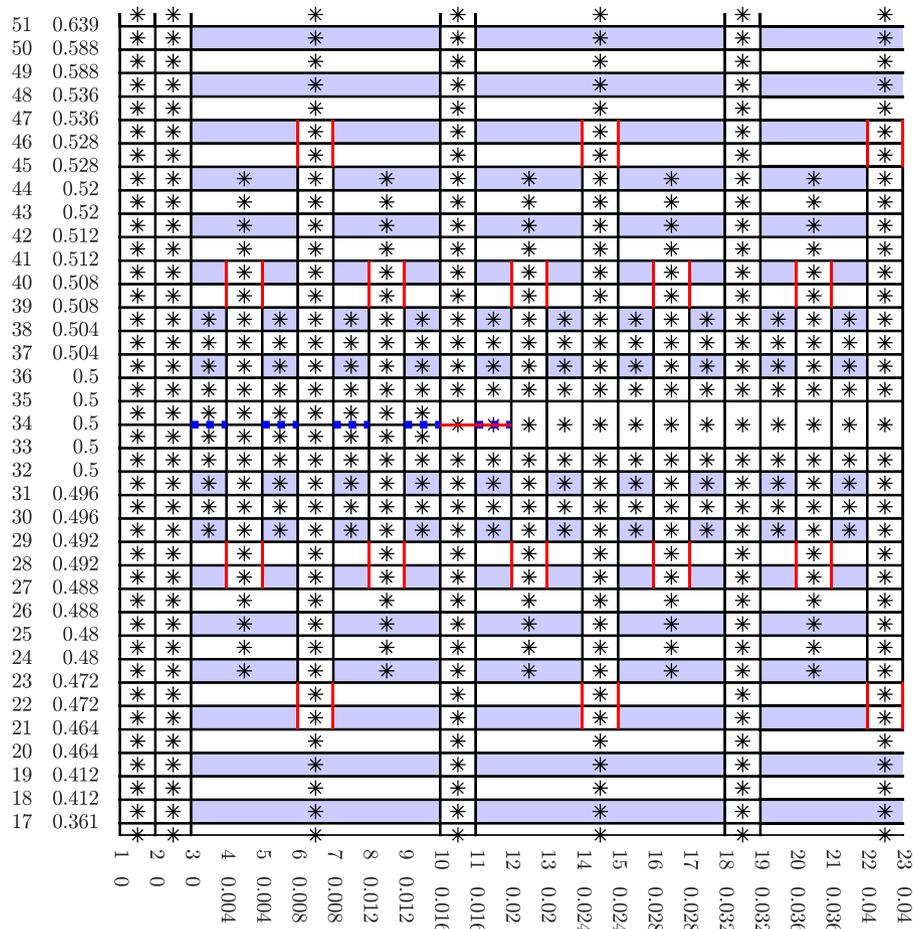
Figure 10 Quartic mesh using the maximum amount of discontinuity lines, as used for the example case.
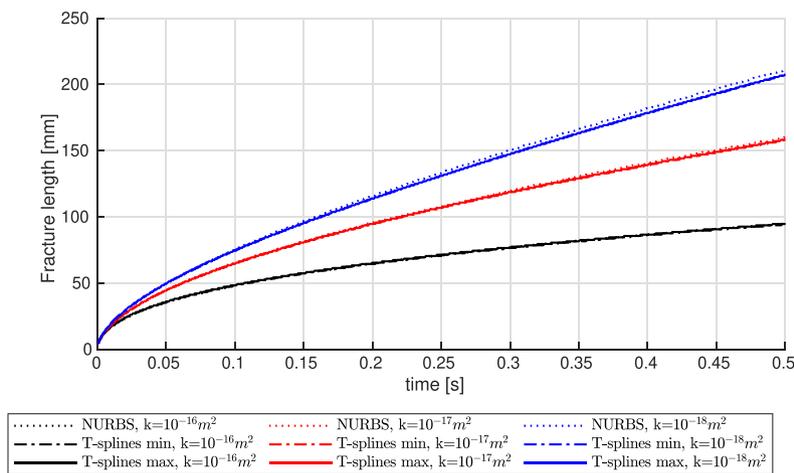
Figure 11 Comparison between the fracture propagation length obtained using the minimal and maximum amount of continuity lines, and a NURBS-based mesh.

differences in opening height for the two elements closest to the fracture tip do not significantly alter the fluid flowing within the fracture. However, the larger opening heights obtained using NURBS allow the fluid to flow more easily through the fracture, increasing the pressure near the crack tip com-

pared to T-splines. This explains the difference between using T-splines and NURBS in propagation velocity for the lower values of the permeability, where the propagation is limited by the pressure and the fluid transport inside the fracture. For the high value of the permeability, propagation is
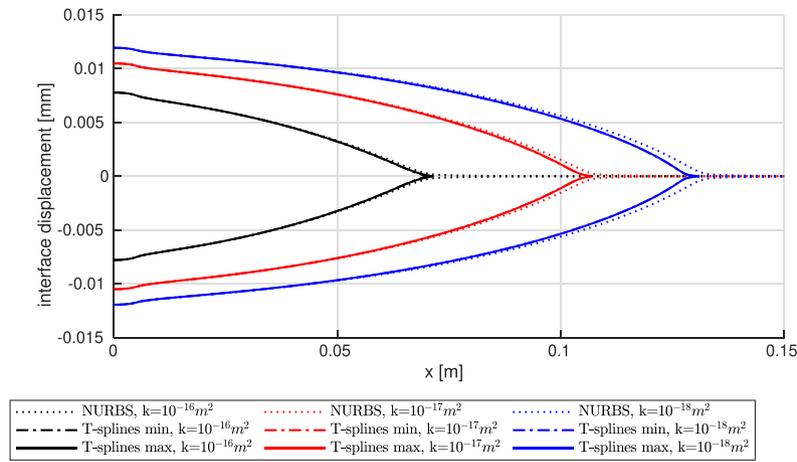
Figure 12 Comparison between the interface displacement at $t = 0.25$ s obtained using the minimal and maximum amount of continuity lines, and a NURBS-based mesh.
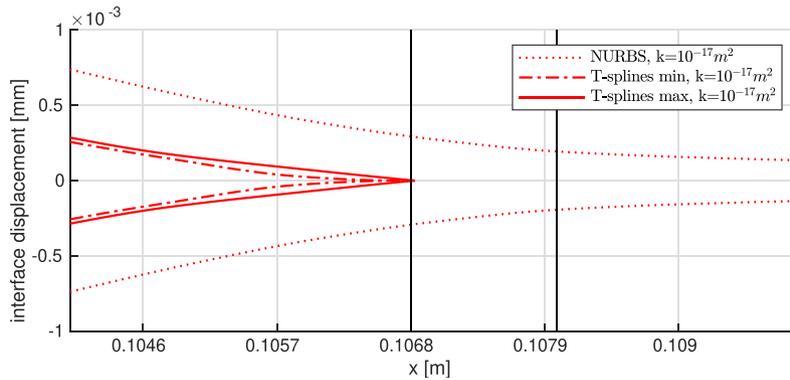
Figure 13 Comparison between the interface displacement at $t = 0.25$ s for the $k = 10^{-17}$ m^2 simulations. The fracture length is indicated with solid black lines.
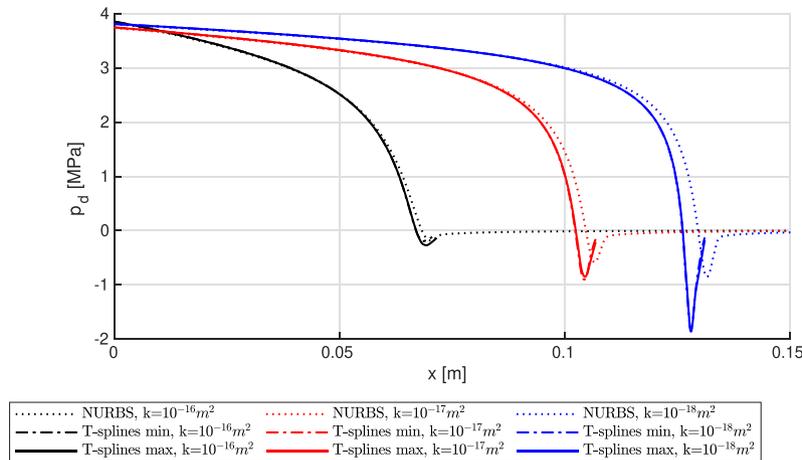
Figure 14 Comparison between the discontinuity pressure at $t = 0.25$ s for the $k = 10^{-17}$ m^2 simulations.

instead limited by the fluid leak-off from the fracture, and therefore this case is less sensitive to the opening height near the crack tip, yielding closer results between NURBS and T-splines.

5. CONCLUSIONS

We have shown how to generate unequal order T-spline meshes. By combining a cubic mesh for the interstitial fluid pressure with a quartic mesh for the solid displacement, the inf-sup

condition can be fulfilled and non-physical pressure oscillations are normally prevented. Interface elements are created to retain the higher-order inter-element continuity, with the interface being described through mesh lines and reduced continuity lines. By propagating this discontinuity along a pre-determined C^0 continuity line, the Bézier extraction operators of the elements remain constant, and the Bézier extraction operator for the newly created interface element could be obtained in a straightforward manner.

Unequal order meshes allow for several choices of the quartic mesh near the discontinuity: either using a minimum amount of mesh lines to match the discontinuity between the two meshes, or adding an extra mesh line to increase the degrees of freedom near the fracture tip. These two choices have been compared, showing near to no difference on the overall results and only slight differences in the fracture opening height close to the crack tip.

Comparing the T-spline meshes with a mesh generated with NURBS, the advantages of T-splines are clear: The T-spline meshes allow for smaller elements near the discontinuity, and larger elements for the remainder of the domain. By contrast, the NURBS mesh requires mesh refinements for the entire domain. Furthermore, T-spline meshes allow using interface elements only for the fracture. Comparing NURBS and T-splines shows that T-splines result in a completely closed fracture at the crack tip, whereas the dummy stiffness used with NURBS yields a slightly open fracture at the crack tip. This difference in fracture opening height alters the discontinuity pressure near the fracture tip, slightly changing the fracture propagation velocity for cases limited by the fluid transport within the fracture. This shows T-splines are not only useful in avoiding the need for interface elements for the intact material, but that using T-splines can result in more correct results when the fluid transport at the crack tip is dominant. However, when fluid leak-off is the dominating mechanism, NURBS and T-splines are equally suitable for simulating fracturing porous materials.

ACKNOWLEDGMENTS

REFERENCES

1. Irzal F, Remmers JJC, Verhoosel CV, de Borst R. Isogeometric finite element analysis of poroelasticity. *International Journal for Numerical and Analytical Methods in Geomechanics*. 2013;**37**:1891–1907.
2. Hageman T, de Borst R. Flow of non-Newtonian fluids in fractured porous media: Isogeometric vs standard finite element discretisation. *International Journal for Numerical and Analytical Methods in Geomechanics*. 2019;**43**:2020–2037.
3. Brezzi F, Fortin M. *Mixed and Hybrid Finite Element Methods*. vol. **15**. New York: Springer, 1991.
4. Chapelle D, Bathe KJ. The inf-sup test. *Computers & Structures*. 1993;**47**:537–545.
5. Krischok A, Linder C. A generalized inf-sup test for multi-field mixed-variational methods. *Computer Methods in Applied Mechanics and Engineering*. 2019;**357**:112497.
6. Dortdivanlioglu B, Krischok A, Beirão da Veiga L, Linder C. Mixed isogeometric analysis of strongly coupled diffusion in porous materials. *International Journal for Numerical Methods in Engineering*. 2018;**114**:28–46.
7. Buffa A, de Falco C, Sangalli G. IsoGeometric analysis: stable elements for the 2D Stokes equation. *International Journal for Numerical Methods in Fluids*. 2011;**65**:1407–1422.
8. Ahn JS, Bluck MJ. Isogeometric analysis of the time-dependent incompressible MHD equations. *International Journal of Computational Fluid Dynamics*. 2020;**34**:226–248.
9. White JA, Borja RI. Stabilized low-order finite elements for coupled solid-deformation/fluid-diffusion and their application to fault zone transients. *Computer Methods in Applied Mechanics and Engineering*. 2008;**197**:4353–4366.
10. Vignollet J, Kaczmarczyk L, Pearce CJ. A Galerkin least-square stabilisation technique for hyperelastic biphasic soft tissue. *Computers & Structures*. 2013;**118**:109–114.
11. Li W, Wei C. Stabilized low-order finite elements for strongly coupled poromechanical problems. *International Journal for Numerical Methods in Engineering*. 2018;**115**:531–548.
12. Hughes TJR, Cottrell JA, Bazilevs Y. Isogeometric analysis: CAD, finite elements, NURBS, exact geometry and mesh refinement. *Computer Methods in Applied Mechanics and Engineering*. 2005;**194**:4135–4195.
13. Vignollet J, May S, de Borst R. On the numerical integration of isogeometric interface elements. *International Journal for Numerical Methods in Engineering*. 2015;**102**:1733–1749.
14. Hageman T, Pervaiz Fathima KM, de Borst R. Isogeometric analysis of fracture propagation in saturated porous media due to a pressurised non-Newtonian fluid. *Computers and Geotechnics*. 2019;**112**:272–283.
15. Hennig P, Müller S, Kästner M. Bézier extraction and adaptive refinement of truncated hierarchical NURBS. *Computer Methods in Applied Mechanics and Engineering*. 2016;**305**:316–339.
16. Kolo I, Chen L, de Borst R. Strain-gradient elasticity and gradient-dependent plasticity with hierarchical refinement of NURBS. *Finite Elements in Analysis and Design*. 2019;**163**:31–43.
17. Chen L, Lingen FJ, de Borst R. Adaptive hierarchical refinement of NURBS in cohesive fracture analysis. *International Journal for Numerical Methods in Engineering*. 2017;**112**:2151–2173.
18. Bazilevs Y, Calo VM, Cottrell JA, Evans JA, Hughes TJR, Lipton S et al., Isogeometric analysis using T-splines. *Computer Methods in Applied Mechanics and Engineering*. 2010;**199**:229–263.
19. Scott MA, Borden MJ, Verhoosel CV, Sederberg TW, Hughes TJR. Isogeometric finite element data structures based on Bézier extraction of T-spline. *International Journal for Numerical Methods in Engineering*. 2011;**88**:126–156.
20. May S, Vignollet J, de Borst R. The role of the Bézier extraction operator for T-splines of arbitrary degree: linear dependencies, partition of unity property, nesting behaviour and local refinement. *International Journal for Numerical Methods in Engineering*. 2015;**103**:547–581.
21. de Borst R, Chen L. The role of Bézier extraction in adaptive isogeometric analysis: local refinement and hierarchical refinement. *International Journal for Numerical Methods in Engineering*. 2018;**113**:999–1019.
22. Chen L, de Borst R. Locally refined T-splines. *International Journal for Numerical Methods in Engineering*. 2018;**114**:637–659.
23. Chen L, Verhoosel CV, de Borst R. Discrete fracture analysis using locally refined T-splines. *International Journal for Numerical Methods in Engineering*. 2018;**116**:117–140.
24. Verhoosel CV, Scott MA, de Borst R, Hughes TJR. An isogeometric approach to cohesive zone modeling. *International Journal for Numerical Methods in Engineering*. 2011;**87**:336–360.
25. Scott MA, Li X, Sederberg TW, Hughes TJR. Local refinement of analysis-suitable T-splines. *Computer Methods in Applied Mechanics and Engineering*. 2012;**213–216**:206–222.

26. Zienkiewicz OC, Chan AHC, Pastor M, Schrefler BA, Shiomi T. *Computational Geomechanics - With Special Reference to Earthquake Engineering*. Chichester: John Wiley & Sons, 1999.

27. de Borst R. *Computational Methods for Fracture in Porous Media*. New York: Elsevier, 2017.

28. Remij EW, Remmers JJC, Huyghe JM, Smeulders DMJ. The enhanced local pressure model for the accurate analysis of fluid pressure driven fracture in porous materials. *Computer Methods in Applied Mechanics and Engineering*. 2015;**286**: 293–312.